Materials Science and Engineering A 528 (2011) 6324–6333

Contents lists available at ScienceDirect

Materials Science and Engineering A

journal homepage: www.elsevier.com/locate/msea

Thermo-mechanical characterization of epoxy/clay nanocomposites as matrices for carbon/nanoclay/epoxy laminates

Andrea Dorigato[a,*], Alessandro Pegoretti[a], Marino Quaresimin[b]

[a] Department of Materials Engineering and Industrial Technologies, University of Trento, via Mesiano 77, 38123 Trento, Italy
[b] Department of Management and Engineering, University of Padova, Stradella S. Nicola 3, 36100 Vicenza, Italy

ARTICLE INFO

Article history:
Received 23 December 2010
Accepted 14 April 2011
Available online 21 April 2011

Keywords:
Mechanical characterization
X-ray diffraction
Composites
Polymers
Nanostructured materials
Fracture

ABSTRACT

Microstructural and thermo-mechanical characterization were performed on epoxy–clay nanocomposites, to be used as matrix for continuous carbon fiber reinforced composites, containing various amounts of clays having different hydrophilicity. XRD tests displayed that the dispersion degree of the clay lamellae was strictly correlated to their hydrophilicity, while DSC tests revealed that the crosslinking degree was negatively affected by the presence of most hydrophilic clays. Therefore, the balance between polymer–filler interaction and crosslinking degree influenced the final properties of the resulting composites. The mechanical behaviour, both under quasi-static and impact conditions, was positively affected by resin nanomodification. Fracture toughness and threshold to crack initiation under cyclic loading were also interestingly improved.

While the effect of nanoclay introduction on the quasi-static tensile properties of the carbon/epoxy laminates was negligible, Charpy impact tests on nanomodified epoxy/carbon fiber cross-ply laminates evidenced slight enhancements of the elastic modulus and of the energy adsorption capacity with respect to the unfilled epoxy–carbon composites. Moreover, drop weight test on laminates evidenced improvements in energy absorption capacity due to resin nanomodification.

1. Introduction

In the last years polymeric nanocomposites attracted the interest of many researchers and industries all over the world, and many works has been published on the thermo-mechanical properties of nanomodified thermoplastic or thermosetting matrices [1,2]. Many kinds of inorganic nanofillers, different for the morphology and the surface properties, were utilized, but the lamellar silicates (montmorillonites) were probably the most investigated [3,4]. These nanofillers are characterized by a lamellar structure, in which every layer, 1 nm thick and 200–300 nm long, is constituted by a central octahedral sheet of alumina or magnesia alternated to two external silica tetrahedrons. These lamellae are stacked together with a regular van der Waals gap between them. Negative charges created by isomorphic substitution within the layers are counterbalanced by Na^+ or Ca^{2+}cations in the interlayer regions. Considering that the forces that keep the stacks together are relatively weak, the intercalation of organic molecules between the lamellae can easily occur [5]. If the hydrated cations of the interlayer are substituted with cationic surfactants such as alkylammonium or alkylphosphonium salts [6–8], organo-modified (OM) clays can be synthesized. Three main types of composites may be obtained when OM clays are added to a polymer liquid, depending on the chemical nature of the modifier and on the preparation process. When polymer chains are unable to penetrate into the silicate sheets, a phase separated microcomposite is formed. Intercalated structure can be obtained when the macromolecules are present in the interlayer galleries of the silicate, resulting in a well ordered multilayer morphology constituted by polymeric and inorganic layers. An exfoliated structure is obtained when the silicate layers are completely and uniformly dispersed in the matrix [9]. Filler–matrix interactions determine dispersion level of the clay in the polymer matrix and the resultant thermo-mechanical behaviour of polymer–clay nanocomposites [10]. Nanoclays are expected to yield improvements over unfilled polymers in a very wide range of properties. Polymer/clay nanocomposites can generally show improvements of the tensile mechanical properties [11,12] and of the fracture resistance [13–16] with respect to the neat polymer. With the nanomodification of polymeric matrices an increase of the dimensional stability and of the barrier properties [17] and a better thermal degradation resistance [18,19] can be easily obtained.

However, the mechanical properties displayed by polymer nanocomposites are much lower than that required to engineering structural materials, such as advanced composites reinforced with high-performance continuous fibers [20]. For this reason in

* Corresponding author. Tel.: +39 0461 882412; fax: +39 0461 881977.
E-mail address: andrea.dorigato@ing.unitn.it (A. Dorigato).

0921-5093/$ – see front matter © 2011 Elsevier B.V. All rights reserved.
doi:10.1016/j.msea.2011.04.042

Table 1
Organoclays used in this study. Information taken from the producer data sheets.

Trade name	Organic modifier	Modifier concentration [meq/100 g clay]	Density [g cm^{-3}]
Cloisite® 30B	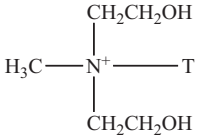	90	1.87
Cloisite® 25A	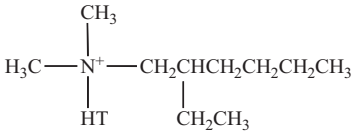	95	1.87
Cloisite® 15A	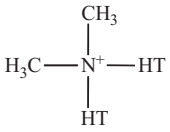	125	1.66

T: Tallow (~65% C18; ~30% C16; ~5% C14) and HT is Hydrogenated Tallow.
Anion: chloride.

the last years rising interest was devoted to the development of ternary composites, in which both traditional continuous high performance micro-fibers and nanofillers are added to a thermosetting [21–26] or a thermoplastic polymer matrix [27,28]. In particular, some attempts have been made to improve the matrix-dominated properties of polymer composites by adding OM clays or carbon nanofibers to the epoxy matrix [29–39].

For example, Bozkurt et al. [31] studied the mechanical and thermal properties of non-crimp glass fiber reinforced clay/epoxy nanocomposites, finding that the flexural properties of laminates were improved by clay addition, because of the improved interface between glass fibers and epoxy. Zhou et al. [39] used a vacuum assisted resin transfer molding (VARTM) process set up to fabricate carbon nanofiber filled carbon/epoxy laminated composites, finding substantial improvements in flexural strength in nanomodified laminates samples. Chowdhury et al. [40] investigated the effects of nanoclay particles on flexural and thermal properties of woven carbon fiber reinforced polymer matrix composites. Interesting enhancements in flexural strength, in the elastic modulus, and in thermomechanical properties were displayed for 2 wt% nanoclay reinforced composites.

In this work, epoxy/clay nanocomposites were prepared by using three different kinds of organo-modified clays. A microstructural characterization was conducted through X-Ray Diffraction (XRD) analysis and ESEM images, in order to determine the role of clay hydrophobicity on its dispersion in the epoxy matrix. DSC tests were then performed, in order to evaluate the influence of the polymer–filler interaction on the cure kinetics of the resin. The influence of the polymer–filler interaction on the tensile properties and on the fracture resistance of the resulting materials under quasi-static, cyclic and impact loading conditions was then analyzed. Epoxy/clay/carbon fiber cross-ply laminates were also prepared by filament winding technique, in order to assess the contribution due to the clay addition on the matrix-controlled properties of fiber-reinforced composites under quasi-static and impact loading conditions.

2. Experimental

2.1. Materials and preparation of the samples

An epoxy resin, supplied by Elantas Camattini® (Collecchio, Italy), was used as matrix. It is constituted by a MC 102 epoxy base (density at 25 °C = 1.20 g cm^{-3}, viscosity at 25 °C = 5500 mPa s), a WH 102 anidrydic hardener (density at 25 °C = 1.16 g cm^{-3}, viscosity at 25 °C = 60 mPa s), and a IG 847 aminic catalyst (density at 25 °C = 1.04 g cm^{-3}, viscosity at 25 °C = 60 mPa s). The base/hardener/catalyst weight ratio was100:93:0.2. Three different organo-modified clays (Cloisite® 30B, 25A and 15A), provided by Southern Clay Products, Inc. (Gonzales, Texas), were used as nanofiller. Table 1 summarizes some of the characteristics of the selected organoclays. According to the producer's selection chart and to a previous work of our group [10], the selected organo-clays could be ranked in the following order of increasing hydrophobicity: 30B < 25A < 15A. For the preparation of ternary composites, T300 epoxy–compatible high strength continuous carbon fibers, supplied by Torayca® (Japan), were used. Single tows constituted by 3000 fibers were used for the filament winding process.

For the preparation of the samples, the clays were dispersed in the hardener for 2 h at 2000 rpm, by using a Dispermat® F1 mechanical mixer. The base and the catalyst were then added and mixed for 1 h at 2000 rpm. Finally, the mixture was degassed at ambient temperature and poured in silicone moulds. A curing cycle of 2 h at 110 °C + 6 h at 140 °C was then conducted. In this way, pure epoxy samples and nanocomposites filled with different clays at two filler contents (2 wt% and 5 wt%) were prepared. The samples were denoted indicating the matrix (Epoxy) and the kind of clay (30B, 10A or 25A), followed by the filler content. As an example, the Epoxy–25A-5 indicates the 5 wt% Cloisite 25A filled nanocomposite.

Considering that Cloisite 25A filled composites showed the best balance between quasi-static and impact properties, this clay was selected for the preparation of epoxy–clay–carbon fiber laminates, with a filler loading of 5 wt%. After the preparation of the liquid resin, single carbon filaments were wound through a Telmec® ALAB 0102 filament winding machine on a square metallic mandrel, 30 cm long. The plates thus obtained were then compacted in a Carver® press by using square teflon sheets as releasing plies and cured with the same thermal cycle applied to epoxy–clay nanocomposites (2 h at 110 °C + 6 h at 140 °C). In this way square symmetric and balanced cross-ply laminates, 20 cm long, were obtained, with a fiber content of about 50 vol%. The lamination sequence was [0/90/0/90/0/90/$\bar{0}$]s. In the results and discussion section, the epoxy/carbon fiber composite was designated as Epoxy–CF, while the 5 wt% Cloisite 25A filled laminate was denoted as Epoxy–25A-5–CF.

2.2. Characterization of epoxy/clay nanocomposites

X-Ray Diffraction analysis was conducted on nanofilled samples, in order to evaluate the dispersion of the clay lamellae in the composites. A Philips Xpert® HRD3000 diffractometer, with a non-monochromatized copper radiation of 1.5406 Å wavelength, an applied voltage of 40 kV and a current of 30 mA, was used. The interlamellar distances of the clay powder (d_0) and of the clays in the composites (d) were evaluated referring to the Bragg's Law. The intercalation degree (ID), representing the increase of the d-spacing with respect to the original interlamellar distance of the clay, was determined as follows:

$$\mathrm{ID} = \left(\frac{d - d_0}{d_0}\right) \times 100 \quad (1)$$

Fracture surfaces of pure epoxy and nanofilled samples, obtained from SENB samples used in flexural tests for the evaluation of the fracture toughness parameters (K_{IC}, G_{IC}), were observed through a Philips XL30 Environmental Scanning Electronic Microscope (ESEM), at an acceleration voltage of 10 kV and a pressure of 93 Pa.

The transparency of the samples was assessed in order to have a qualitative evaluation of the dispersion degree of the clay nanoplatelets. Some photographs of pure epoxy and of the nanofilled samples (thickness = 4 mm) were taken by using a Nikon Coolpix 4500 digital camera. The distance between the camera and the samples was kept constant at 300 mm.

Differential Scanning Calorimetry (DSC) tests were conducted by using a Mettler DSC30 machine on liquid resins. The first thermal cycle, from 30 °C to 270 °C under a nitrogen flow of 100 ml min^{-1}, highlighted the effect of the clay addition on the cure kinetics of the resin. The sample were then cooled at ambient temperature at 10 °C min^{-1}, and then heated again at 270 °C with an heating rate of 10 °C min^{-1}. In this way it was possible to evaluate the influence of the nanofiller on the glass transition temperature (T_g) of the cured resin.

Quasi-static tensile properties were determined by using an Instron 4502 electromechanical tensile testing machine, at a crosshead speed of 1 mm min^{-1}. ISO-527 1B dogbone samples, with a gage length of 50 mm, a width of 10 mm and a thickness of 4 mm, were used. The deformations were evaluated through an Instron 2620-601 extensometer, with a gage length of 50 mm, until a deformation of 1% was reached. Higher deformation levels were recorder referring to the crosshead displacement. The elastic modulus (E) was evaluated according to ISO 527 standards, as secant modulus between the stresses associated to the deformations of 0.05% and of 0.25%. The tests were conducted at ambient temperature (25 °C), and at least five samples were tested for each composition. Three point flexure tests for the evaluation of K_{IC} and G_{IC} parameters were conducted according to ASTMD 5045 standard on SENB samples, 44 mm long, 10 mm wide and 4 mm thick, with a nominal notch of about 5 mm. A crosshead speed of 10 mm min^{-1} was imposed to the samples. At least five tests were performed for each composition.

Charpy impact tests were carried on by using a Ceast® machine on SENB samples, 44 mm long, 10 mm wide and 4 mm thick, with a notch length of 1 mm. An impact speed of 0.5 m s^{-1} and an initial impact angle of 19.5° were set. In this way the specific energy adsorbed at failure, K_{IC} and G_{IC} parameters under impact conditions were determined. For comparative purposes, mode I K_{IC} tests according to ASTM 5045 were carried out. The mode I fatigue behaviour of a reduced selection of materials (neat epoxy and 2 wt% Cloisite 25A filled nanocomposite) was also investigated on CT samples. Both static and fatigue Mode I tests were carried out on a MTS 858 machine. Fatigue tests were carried out under load control, by applying a cyclic sinusoidal load wave with a frequency of 5 Hz and monitoring the crack length evolution along the fatigue life by a travelling microscope.

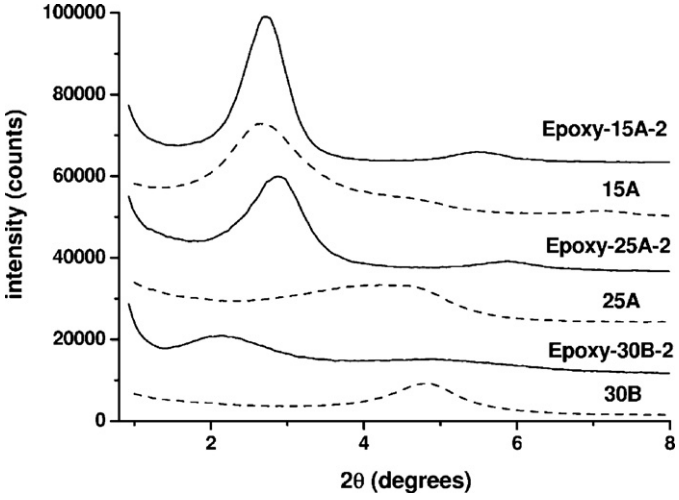

Fig. 1. X-Ray diffractograms of Cloisite clays (dashed lines) and epoxy–2 wt% clay filled nanocomposites (continuous lines).

2.3. Tensile and impact behaviour of epoxy/clay/carbon fiber laminates

Quasi-static tensile tests were carried on by using an Instron 8516 tensile testing machine, according to ASTM D3039 standard. Rectangular samples, 20 mm wide and with a distance between the grips of 80 mm, were used. The deformations were evaluated through an Instron 2620-601 extensometer. Thin rectangular steal sheets were applied to the grips, in order to favour the clamping of the sample. The tests were conducted at room temperature on at least five specimens for each condition. In this way the elastic modulus (E) and the tensile properties at failure (σ_b, ε_b) were calculated. Charpy impact tests were conducted by using a Ceast impact machine on rectangular samples, 80 mm long and 10 cm high, with a span length of 40 mm. An impact speed of 0.5 m s^{-1} and an initial angle of 8° were set. Even in this case, at least five specimens were tested for each condition. The specific energy adsorbed at crack initiation and at break was thus evaluated. Drop weight impact tests on laminates were carried on a Ceast Fractovis Plus 7525 machine, according to ASTM D5628 standard. Square samples, 100 by 100 mm, were tested at room temperature. A tup in geometry FE, having a diameter of 20 mm, equipped with a piezoelectric strain gage and connected to a mass of 10 kg, was used. The specimens were clamped with an annular clamp, with an inside diameter of 40 mm. The specific penetration energy was first measured. Then, a second set of tests was carried out with the aim to quantify and compare the energy absorption capability of laminates made with a nanomodified resin. For this second set of test, the impact energy level was chosen as the 50% of relevant penetration energy.

3. Results and discussion

3.1. Microstructural characterization of epoxy/clay nanocomposites

In Fig. 1 representative X-Ray diffractograms of clay powders and 2 wt% filled nanocomposites are reported, while in Table 2 the most important results are summarized. For all the tested samples it is evident the presence of a diffraction peak, suggesting that the original crystalline order of clay lamellae is totally or partially main-

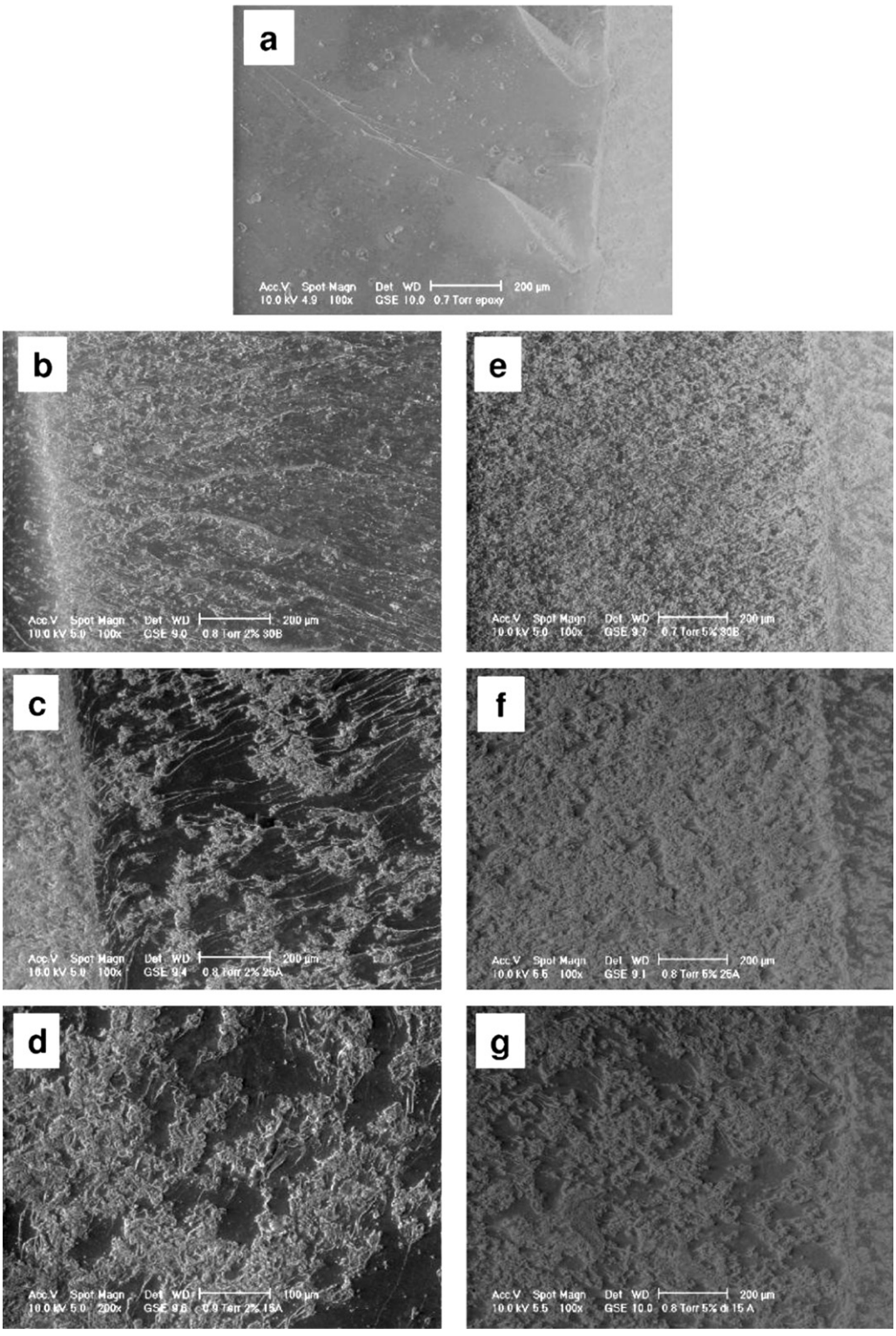

Fig. 2. ESEM images of fracture surfaces of epoxy/clay nanocomposites. (a) Epoxy, (b) Epoxy–30B-2, (c) Epoxy–25A-2, (d) Epoxy–15A-2, (e) Epoxy–30B-5, (f) Epoxy–25A-5, (g) Epoxy–15A-5.

tained. The intensity of this peak is inversely proportional to clay hydrophilicity. This means that in the case of 30B filled composites only a small portion of clay lamellae is stacked together forming crystalline basal planes. Moreover, the shift of the diffraction peaks towards lower angles indicates that all the prepared composites are characterized by an intercalated structure, with an increase of the interlamellar spacing with respect to the original clay powders. In some papers on the microstructural characterization of epoxy–clay nanocomposites a complete exfoliation of the clay lamellae was obtained [41], but the formation of an intercalated structure was more frequently reported in literature [3,14,24,42–46]. Considering the intercalation degree of the composites at the same filler content, it can be noticed that the most hydrophilic clays (30B) presents the maximum enhancement of *d*-spacing, while a very

Table 2
Interplanar distances of Cloisite® clays and relative intercalation degree (ID) of epoxy–clay nanocomposites.

Sample	d_{001} (Å)	d_{001} clay (Å)	ID (%)
Epoxy–30B-2	41.54	18.50	124.5
Epoxy–25A-2	30.71	19.04	61.3
Epoxy–15A-2	32.40	30.98	4.6
Epoxy–30B-5	44.70	18.50	141.6
Epoxy–25A-5	30.18	19.04	58.5
Epoxy–15A-5	33.63	30.98	8.6

low intercalation can be obtained by using relatively hydrophobic clays. It is also evident that the intercalation degree is not influenced by the filler content. This result is in agreement with the observations reported in a previous work on PU-clay nanocomposites [10], in which the intercalation degree resulted proportional to clay hydrophilicity. This means that polymer–filler interactions are probably more intense by using relatively hydrophilic clay (30B), while only weak physical interactions can be registered for the composites filled with hydrophobic clays (15A).

In Fig. 2 ESEM images of the fracture surfaces of pure epoxy and relative nanocomposites are reported. It is immediately evident that the fracture profile of the pure epoxy sample is very smooth, while nanofilled samples present a high degree of surface corrugation, proportionally to the filler content. Taking into account XRD diffractograms reported in Fig. 1, it is not possible to assess if the surface corrugation is due to the presence of stacked clay lamellae or to aggregates formed by clay nanoplatelets. However, the corrugation of the fracture surface due to the presence of clay nanoplatelets is well known in literature [14,43,47], and the creation of a larger fracture surface is generally considered as a positive contribution to the fracture toughness of the material. Furthermore, if composites filled with different clays at the same filler loading are compared, it can be easily noticed that Cloisite 30B filled samples are characterized by the highest surface corrugation degree. This is another indication of the fact that probably in Cloisite 30B filled samples clay lamellae are dispersed more finely with respect to Cloisite 25A and to Cloisite 15A filled composites, probably because of a better polymer–filler interaction.

In Fig. 3 photographs of pure epoxy and nanocomposites samples are reported. It can be easily noticed that the transparency of the unfilled matrix is substantially maintained even at high filler loadings, indicating that a good dispersion of the clay nanoplatelets is reached for all the samples. A slight loss of transparency can be detected for composites filled with higher clay amount (5 wt%),

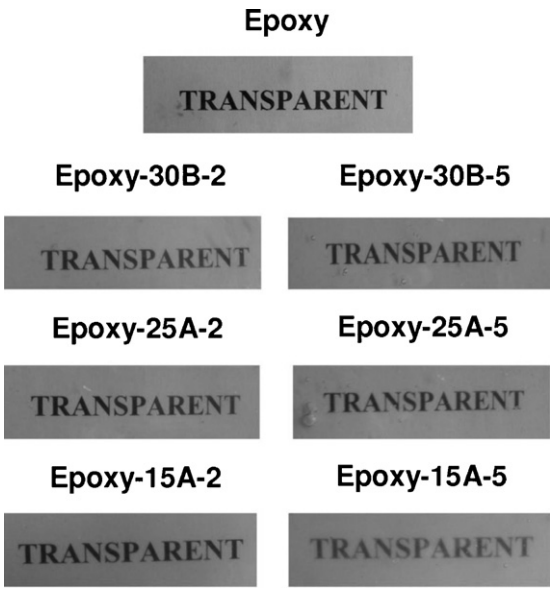

Fig. 3. Photographs of pure epoxy and epoxy/clay nanocomposite samples.

especially increasing the clay hydrophobicity (15A filled nanocomposites). This is probably correlated to the low intercalation degree of 15A filled composites registered in XRD tests.

3.2. Thermo-mechanical properties of epoxy/clay nanocomposites

In Fig. 4a representative DSC curves of pure epoxy and relative 5 wt% filled composites nanocomposites before the crosslinking process are represented, while in Fig. 4b thermograms referred to crosslinked materials are reported. The most important results are summarized in Table 3. It can be observed that the introduction of nanoclay in these systems leads to a slight lowering of the crosslinking temperature, with a shift of the crosslinking peaks to lower temperatures, proportionally to the filler content. Another important aspect is that the presence of nanoclay negatively affects the crosslinking degree of the system, with a general decrease of the crosslinking enthalpy. Interestingly, only Epoxy–15A-5 composite displays a slight enhancement of the crosslinking enthalpy with respect to the pure matrix. On the other hand, XRD test evidenced a very low intercalation degree for this sample, accompanied by a limited polymer–filler interaction. Also glass transition

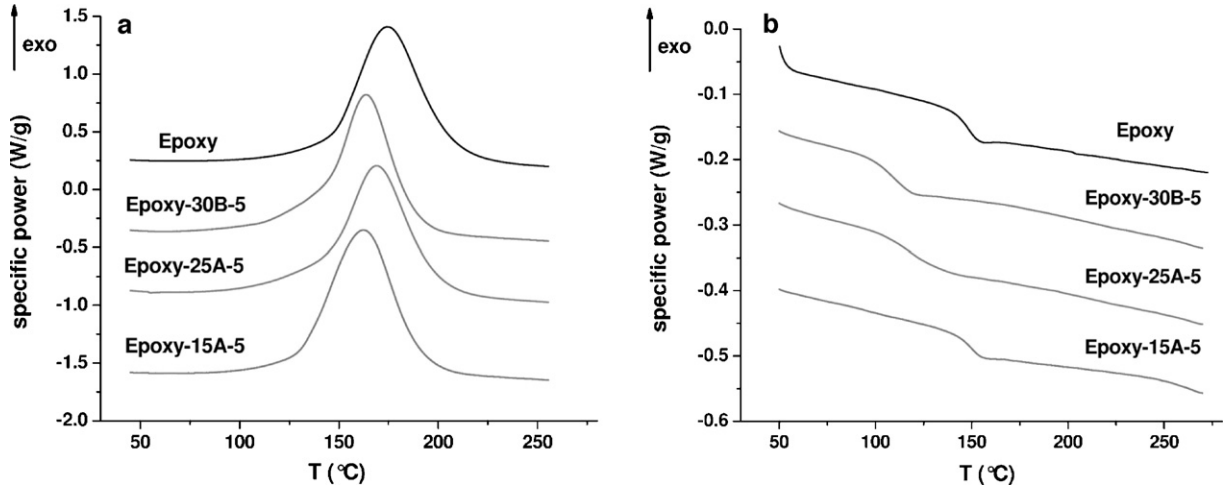

Fig. 4. (a) DSC curves of epoxy/clay nanocomposites (5 wt% samples). First scan. (b) DSC curves of epoxy/clay nanocomposites (5 wt% samples). Second scan.

Table 3
DSC data of epoxy/clay nanocomposites.

Sample	Crosslinking peak (°C)	Crosslinking enthalpy (J g^{-1})	T_g (°C)
Epoxy	174.5	299.0	150.6
Epoxy–30B-2	171.2	276.3	134.4
Epoxy–25A-2	174.7	272.0	147.0
Epoxy–15A-2	171.9	272.9	150.6
Epoxy–30B-5	167.9	268.5	107.6
Epoxy–25A-5	172.6	280.0	118.8
Epoxy–15A-5	165.5	308.4	149.2

Table 4
Quasi-static tensile properties of epoxy/clay nanocomposites.

Sample	E (GPa)	σ_r (MPa)	ε_r (%)
Epoxy	2.87 ± 0.18	27.7 ± 1.6	1.02 ± 0.05
Epoxy–30B-2	2.96 ± 0.21	22.8 ± 1.3	0.77 ± 0.06
Epoxy–25A-2	2.92 ± 0.19	31.8 ± 5.0	1.19 ± 0.26
Epoxy–15A-2	2.86 ± 0.12	23.0 ± 1.8	0.81 ± 0.08
Epoxy–30B-5	3.25 ± 0.23	20.0 ± 3.9	0.63 ± 0.14
Epoxy–25A-5	3.27 ± 0.28	21.8 ± 2.3	0.69 ± 0.09
Epoxy–15A-5	3.06 ± 0.20	26.1 ± 2.8	0.90 ± 0.12

temperature (T_g) of the cured composites is lowered by the nanoclay addition, proportionally to the filler content. The decrease of the glass transition temperature in nanofilled systems, especially at high filler contents, was already reported by other authors in literature [48–50]. Moreover, T_g drop is evident by using hydrophilic clays (30B), while for 15A filled composites the decrease of the glass transition temperature is practically negligible. As already reported in a previous work [10], the different behaviour shown by composites filled with different clays can be explained on the basis of a different polymer–filler interfacial interaction. From XRD tests it was concluded that utilizing a relatively hydrophilic clay (30B), the relative intercalation increases. Consequently, more and more chain extender-cross-linker is probably segregated between the interlamellar galleries of the clays, where it can be hardly reached by the epoxy base oligomers. Therefore, the presence of some unreacted chain extender-cross-linker could explain the lower cross-linking degree and its trend with the intercalation degree. Another possible hypothesis is that a small part the epoxy base might react with the hydroxyl groups and/or with the counterions of clays, thus reducing the amount of oligomer available for crosslinking reactions with the chain extender-cross-linker component [51,52]. Comparing the results from XRD and DSC tests, it can be concluded that polymer–filler interaction promotes the dispersion of the clay nanoplatelets in the matrix but hinders the crosslinking degree of the materials. The balance between these two aspects might have important consequences on the mechanical properties of the resulting composites.

Representative curves of quasi-static tensile tests on pure epoxy resin and Cloisite 25A filled nanocomposites are reported in Fig. 5, while the most important results are summarized in Table 4. It is evident that the elastic modulus is positively affected by the presence of nanoclay, especially at higher filler loading. A similar trend of the elastic modulus was already reported by other authors for epoxy–clay nanocomposite systems [3,44,45,49]. Considering 2 wt% filled samples, the highest elastic modulus is obtained for 30B filled composites, probably because the relatively intense polymer–filler interaction leads to a better dispersion of the clay nanoplatelets. Increasing the filler content, the highest stiffness is registered for 25A filled composites. Even if the differences between the elastic modulus of 30B and 25A filled samples are not so pronounced, it is possible that at relatively high filler loading the positive effect of the matrix-filler interaction is counterbalanced by the decrease of the crosslinking degree. For this reason the highest elastic properties are obtained with Cloisite 25A, an intermediate hydrophobicity clay. In terms of tensile properties, the introduction of the clay leads to a slight decrease of the tensile strength (σ_b) values. Also the strain to failure (ε_b) is negatively affected by the clay addition, especially increasing the filler loading. According to some authors [11,43,53], it is likely that the presence of a fraction of non-intercalated clay tactoids with micrometric dimension acts as crack nucleation sites, with detrimental effects on the tensile properties. However, the drop in tensile strength and strain to failure values registered for nanoclay filled samples is not so significant and this is in agreement with the results reported on several papers dealing with the tensile properties of nanofilled epoxy systems [3,44,49].

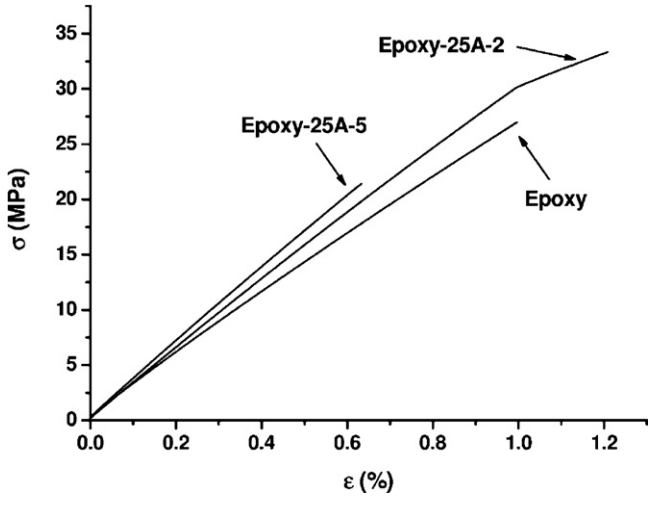

Fig. 5. Representative quasi-static tensile tests on pure epoxy and Cloisite 25A filled nanocomposites.

An opposite trend is instead displayed by nanofilled samples when flexural tests for the evaluation of the fracture toughness are considered. Fig. 6a shows representative force–displacement curves of pure epoxy and relevant nanocomposites obtained from flexural tests on notched samples, while in Fig. 6b and c K_{IC} and G_{IC} values of epoxy–clay nanocomposites are reported. An increase of K_{IC} values with the filler content can be generally detected for the nanofilled samples. Even in this case at low filler content (2 wt%) the most important enhancement of the fracture toughness is obtained for 30B filled sample, because of the better polymer filler interaction, while at higher clay loadings (5 wt%) the best performances are displayed by 25A filled composites. The enhancement of the crack propagation resistance is even more pronounced if G_{IC} values are considered. As an example, G_{IC} of Epoxy–15A-5 nanocomposite is about three times higher than that of the pure epoxy matrix. It is worthwhile to note that comparable increments of the fracture toughness have been already reported in the scientific literature on epoxy–clay nanocomposites [14,54]. If in quasi-static tensile tests on un-notched samples the presence of clay aggregates is responsible of the stress concentration and of the crack nucleation, it could be hypothesized that when a notch is already present on the sample the embrittling effect due to agglomerates is not effective and other mechanisms can be responsible of the toughening effect encountered for nanofilled samples. Considering that the dimensions of individual clay nanoplatelets are probably too small to produce an appreciable crack deflection within the matrix, it could be tentatively hypothesized that the presence of aggregates formed by stacked clay lamellae effectively modify the crack propagation path, with positive effects on the fracture toughness of the material. Unfortunately, ESEM images reported in Fig. 2 are not helpful in this sense, and the presence of stacked nanoplatelets in the samples could be definitely assessed only by TEM images.

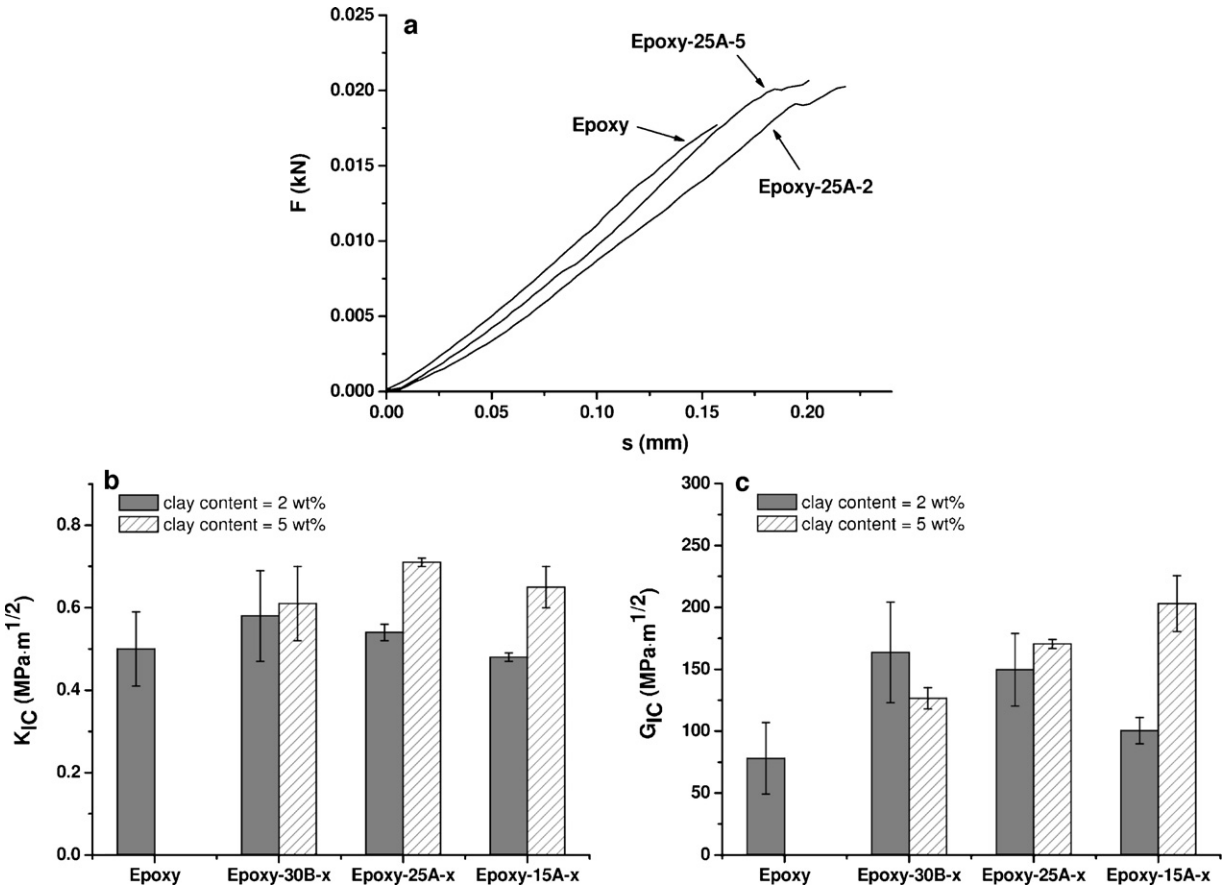

Fig. 6. (a) Fracture toughness of epoxy/clay nanocomposites from SENB tests under quasi-static conditions. Representative force–displacement curves. (b) Fracture toughness of epoxy/clay nanocomposites from SENB tests under quasi-static conditions. K_{IC}. (c) Fracture toughness of epoxy/clay nanocomposites from SENB tests under quasi-static conditions. G_{IC}.

Mode I tests on CT samples provide comparable results in terms of both values and trends. Similar results can be also found with the analysis of the fracture behaviour of neat epoxy and nanocomposite samples under impact conditions. Fig. 7a shows representative force–time curves of pure epoxy and 25A filled composites, while in Fig. 7b and in Fig. 7c K_{IC} and G_{IC} values are respectively reported. Finally, in Fig. 7d specific energy at break values are summarized. Even in this case an interesting enhancement of the fracture toughness due to nanoclay addition can be easily detected. At low filler content the best performances are displayed by 30B filled composites, increasing the filler loading 25A filled composites show the maximum K_{IC} and G_{IC} values. As an example, G_{IC} of Epoxy–30B-2 composite is three times higher than that of the neat resin. The same considerations hold for the analysis of the specific adsorbed energy values.

Results of Mode I fatigue testing on neat epoxy and 2 wt% Cloisite 25A nanocomposite samples are presented in Fig. 8. The position of the curves for the nanomodified epoxy in the right hand side of the plot clearly indicates a significant improvement in the threshold for crack initiation due to the clay addition. The resistance to crack propagation, quantified by the slopes of the curves, seems instead to be unaffected. In any case, further data and analyses are required to provide statistically meaningful conclusions on this point as well as to identify the mechanisms responsible to this specific behaviour.

On the basis of an overall analysis of the results discussed above, it can be concluded that the introduction of clay in these systems leads to an interesting enhancement of the fracture toughness of the material, both under quasi-static cyclic and impact loading conditions.

3.3. Tensile and impact behaviour of epoxy/clay/carbon fiber laminates

In Table 5 quasi-static tensile properties of epoxy/carbon fiber and epoxy/carbon fiber/clay laminates are summarized. Considering standard deviations, it can be concluded that the addition of nanoclay in these systems leads to slight or negligible enhancements of the elastic modulus with respect to the epoxy/carbon fiber laminate, and also the stress at break is practically unaffected by nanoclay introduction. Only a slight increase of the deformation at break can be detected. The reported results are in agreement with many literature references on the tensile behaviour of nanomodified epoxy–clay laminates. Siddiqui et al. [23], Timmerman et al. [55] and Rice et al. [38], studying quasi-static properties of carbon fiber reinforced epoxy–clay laminates, found that the elastic modulus was little improved or unaffected by the presence of nanoclay, while tensile stress was marginally reduced with the nanofiller content. On the other hand, Chowdhury et al. [40] found slight improvements both of the strength and of the modulus by adding 2 wt% organoclay to epoxy–carbon fiber composites. Considering that longitudinal properties of high performance composites are mainly determined by the reinforcement, it is clear that the slight

Table 5
Quasi-static tensile properties of epoxy/carbon fiber and epoxy/carbon fiber/clay laminates.

Sample	E (GPa)	σ_r (MPa)	ε_r (%)
Epoxy–CF	54.0 ± 13.0	526 ± 60	2.3 ± 0.9
Epoxy–25A-5-CF	60.3 ± 7.4	534 ± 34	3.3 ± 0.8

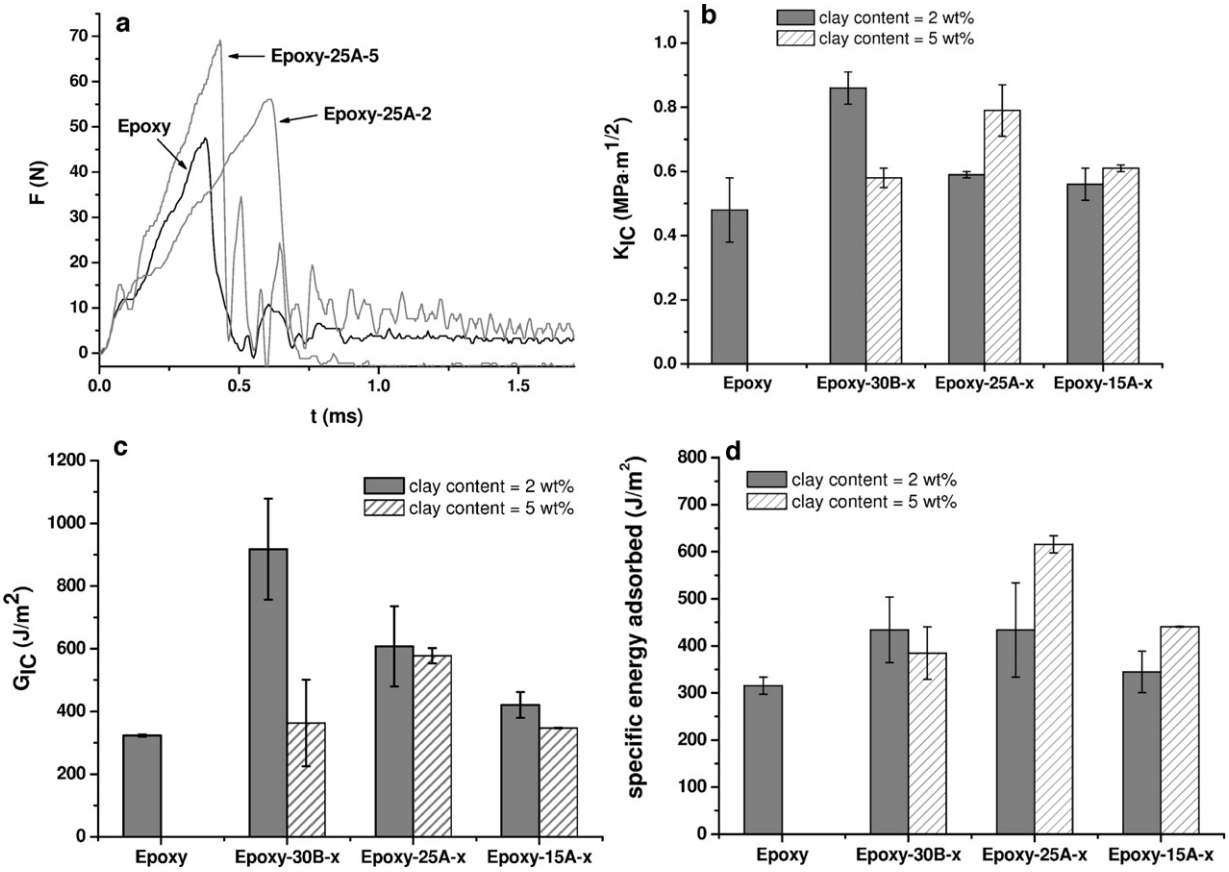

Fig. 7. (a) Charpy impact tests on epoxy/clay nanocomposites. Force–time representative curves. (b) Charpy impact tests on epoxy/clay nanocomposites. K_{IC}. (c) Charpy impact tests on epoxy/clay nanocomposites. G_{IC}. (d) Charpy impact tests on epoxy/clay nanocomposites. Specific energy adsorbed at break.

improving effect on the mechanical properties of the matrix due to nanoclay introduction can only marginally affect the quasi-static tensile behaviour of the material. The little difference in the elastic modulus between neat resin and nanofilled laminate can be also partly attributed to possible fiber misalignments during the fibers winding or the subsequent curing process.

Results for Charpy impact tests on unnotched laminates are shown in Fig. 9a, where representative force–time curves are reported. Fig. 9b shows instead the specific energy adsorbed at crack initiation and at complete failure. The amount of energy adsorbed at crack initiation is not influenced by nanoclay addition, while a slight improvement can be detected if the energy adsorbed at failure is considered. This probably means that the toughening effect provided by clay nanoplatelets is effective during the second part of test when, after initiation the damage propagates and the dissipative mechanisms are actived.

These conclusions are confirmed, even though from a slightly different point of view, by the results deriving from drop weight tests. These results, are shown in Fig. 10 where the values of the specific energy adsorbed during impact by neat epoxy and clay modified laminates are presented. Energy values are normalised by the thickness raised to 1.5 to properly account for the different thickness of the laminates. When the available impact energy is larger than the penetration threshold, the maximum value of the absorbed energy is indeed the penetration energy. As one can expect, being the penetration energy mainly controlled by the fiber strength, there is only a limited influence of the nanomodification. This results in an increase of the penetration energy for nanomodified laminates of 4% only, also in the presence of a significant scatter. On the other hand, a rather different behaviour is observed if the available energy impact is lower than that required to penetrate the laminate. In this case, after the impact, the striker rebounds: part of the impact energy is absorbed, inducing damage in the laminate in the form of matrix cracking, delamination and fiber failures, and the remaining is released as rebound energy. For non penetrating impact test, the damage mechanisms activated are mainly controlled by the matrix properties and, in this condition, the contribution of the nanomodification to the capability of the laminate to absorb energy is clearly evident. There is in fact an increase in the specific absorption capability of about 26% (associated to a very limited scatter) for the nanomodified laminates when compared to the neat epoxy laminates.

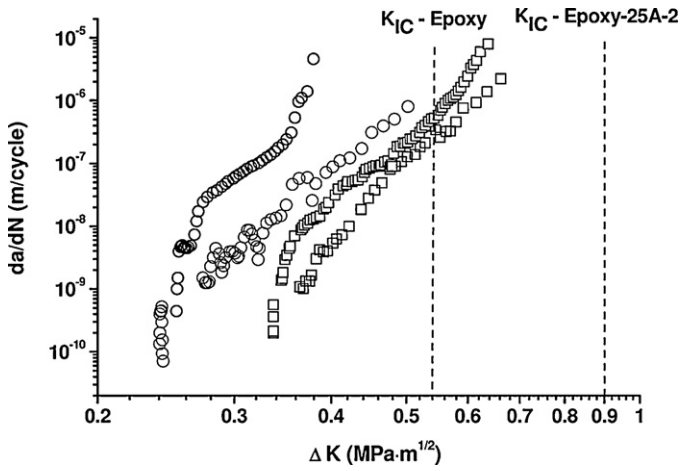

Fig. 8. Mode I fatigue plots of (○) Epoxy and (□) Epoxy–25A-2 nanocomposite.

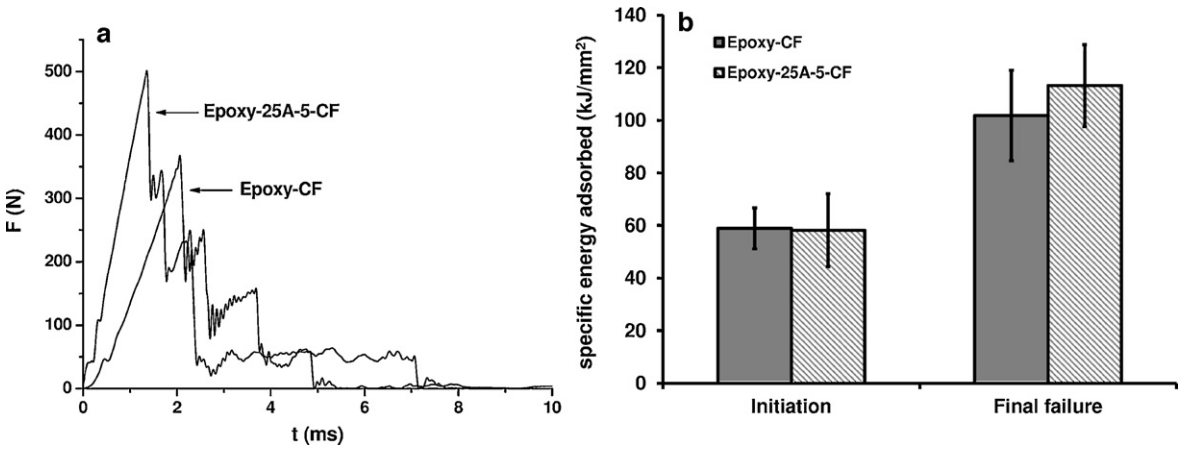

Fig. 9. (a) Charpy impact tests on epoxy/carbon fiber and epoxy/carbon fiber/clay laminates. Representative force–time curves. (b) Charpy impact tests on epoxy/carbon fiber and epoxy/carbon fiber/clay laminates. Specific energy adsorbed at crack initiation and at complete failure.

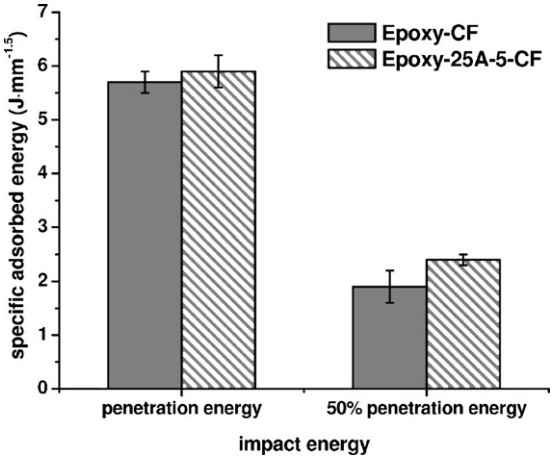

Fig. 10. Specific energy adsorbed by epoxy/carbon fiber and epoxy/carbon fiber/clay laminates in drop weight tests.

4. Conclusions

Epoxy–clay nanocomposites, to be used as matrix for the preparation of carbon fiber reinforced composite materials, were prepared and thermo-mechanically characterized. Three kind of clay at different filler contents were utilized. XRD tests revealed the formation of an intercalated structure for all the samples, increasing the dispersion degree of the clay nanoplatelets with the clay hydrophilicity, while DSC tests evidenced that the crosslinking process was negatively affected by nanoclay addition, especially for hydrophilic clays. Therefore, the resulting mechanical properties were determined by a balance between polymer–filler interaction and crosslinking degree. The mechanical behaviour under quasi-static, impact and fatigue loadings was positively affected by resin nanomodification, and also the fracture toughness was greatly improved.

Introduction of Cloisite 25A in epoxy–carbon fiber cross-ply laminates produced a slight improvement of the tensile properties with respect to the unfilled epoxy–carbon composites, especially under impact conditions. Furthermore, a significant improvement in the energy absorption capability of the laminates due to resin nanomodification was detected in drop weight tests.

References

[1] D.R. Paul, L.M. Robeson, Polymer 49 (2008) 3187–3204.
[2] S. Pavlidou, C.D. Papaspyrides, Progress in Polymer Science 33 (2008) 1119–1198.
[3] C. Basara, U. Yilmazer, G. Bayram, Wiley Interscience (2005).
[4] E.P. Giannelis, R. Krishnamoorti, E. Manias, Advances in Polymer Science 118 (1999) 108–147.
[5] B.K.G. Theng, The Chemistry of Clay-Organic Reactions, Adam Hilger Ltd., London, 1974.
[6] L. Kovarova, A. Kalendova, J.F. Gerard, J. Malac, J. Simonik, Z. Weiss, Macromolecular Symposia 221 (2005) 105–114.
[7] T. Peprnicek, J. Duchet, L. Kovarova, J. Malac, J.F. Gerard, J. Simonik, Polymer Degradation and Stability 91 (2006) 1855–1860.
[8] T. Peprnicek, A. Kalendova, E. Pavlova, J. Simonik, J. Duchet, J.F. Gerard, Polymer Degradation and Stability 91 (2006) 3322–3329.
[9] Song, Y. Hu, Y. Tang, R. Zhang, R. Chen, W. Fan, Polymer Degradation and Stability 87 (2005) 111–116.
[10] A. Pegoretti, A. Dorigato, M. Brugnara, A. Penati, European Polymer Journal 44 (2008) 1662–1672.
[11] I. Isik, U. Yilmazer, G. Bayram, Polymer 44 (2003) 6371–6377.
[12] J.C. Lin, L. Chang, M.H. Nien, H.L. Ho, Composite Structures 74 (2006) 30–36.
[13] S. Avlar, Y. Qiao, Composites A 36 (2005) 624–630.
[14] W. Liu, S.V. Hoa, M. Pugh, Composites Science and Technology 65 (2005) 2364–2373.
[15] G. Ragosta, M. Abbate, P. Musto, G. Scarinzi, L. Mascia, Polymer 46 (2005) 10506–10516.
[16] X.F. Yao, H.Y. Yeh, H.P. Zhao, Journal of Composite Materials 39 (2005) 1487–1496.
[17] J.K. Kim, C. Hu, R.S.C. Woo, M.L. Sham, Composites Science and Technology 65 (2005) 805–813.
[18] S. Varghese, K.G. Gatos, A.A. Apostolov, J. Karger-Kocsis, Journal of Applied Polymer Science 92 (2004) 543–551.
[19] J. Zhang, D.D. Jiang, C.A. Wilkie, Polymer Degradation and Stability 91 (2005) 358–366.
[20] Y. Dzenis, Science 319 (2008) 419–420.
[21] X. Kornmann, M. Rees, Y. Thomann, A. Necola, M. Barbezat, R. Thomann, Composites Science and Technology 65 (2005) 2259–2268.
[22] L.Y. Lin, J.H. Lee, C.E. Hong, G.H. Yoo, S.G. Advani, Composites Science and Technology 66 (2006) 2116–2125.
[23] N.A. Siddiqui, R.S.C. Woo, J.K. Kim, C.C.K. Leung, A. Munir, Composites A 38 (2007) 449–460.
[24] A.K. Subramaniyan, C.T. Sun, Composites Part a-Applied Science and Manufacturing 37 (2006) 2257–2268.
[25] M.H.G. Wichmann, J. Sumfleth, F.H. Gojny, M. Quaresimin, B. Fiedler, K. Schulte, Engineering Fracture Mechanics 73 (2006) 2346–2359.
[26] M. Quaresimin, R.J. Varley, Composites Science and Technology 3–4 (2008) 718–726.
[27] D.P.N. Vlasveld, H.E.N. Bersee, S.J. Picken, Polymer 46 (2005) 10269–10278.
[28] D.P.N. Vlasveld, W. Daud, H.E.N. Bersee, S.J. Picken, Composites A 38 (2007) 730–738.
[29] L. Aktas, Y.K. Hamidi, M.C. Altan, Plastics Rubber and Composites 33 (2004) 267.
[30] O. Becker, R.J. Varley, J.P. Simon, Journal of Materials Science Letters 22 (2003) 1411.
[31] E. Bozkurt, E. Kaya, M. Tanoglu, Composites Science and Technology 67 (2007) 3394–3403.
[32] C. Chen, D. Curliss, SAMPE Journal 37 (2001) 11.
[33] A. Haque, M. Shamsuzzoha, F. Hussain, D. Dean, Journal of Composite Materials 37 (2003) 1821.
[34] M. Hussain, A. Nakahira, K. Niihara, Materials Letters 26 (1996) 185.
[35] M.H.R. Jen, Y.C. Tseng, C.H. Wu, Composites Science and Technology 65 (2005) 775.

[36] S.A. Meguid, Y. Sun, Materials & Design 25 (2004) 289.
[37] H. Miyagawa, R.J. Jurek, A.K. Mohanty, M. Misra, L.T. Drzal, Composites Part a-Applied Science and Manufacturing 37 (2006) 54.
[38] B.P. Rice, C. Chen, L. Cloos, D. Curliss, SAMPE Journal 37 (2001) 7.
[39] Y. Zhou, F. Pervin, V.K. Rangari, S. Jeelani, Materials Science Engineering A 426 (2006) 221–228.
[40] F.H. Chowdhury, M.V. Hosur, S. Jeelani, Materials Science Engineering A 421 (2006) 298–306.
[41] Y. Ke, J. Lu, X. Yi, J. Zhao, Z. Qi, Journal of Applied Polymer Science 78 (2000) 808–815.
[42] M. Abdel-Goad, P. Potschke, Journal of Non-Newtonian Fluid Mechanics 128 (2005) 2–6.
[43] B. Akbari, R. Bagheri, European Polymer Journal 43 (2007) 782–788.
[44] S. Benfarhi, C. Decker, L. Keller, K. Zahouily, European Polymer Journal 40 (2004) 493–501.
[45] D. Dean, R. Walker, M. Theodore, E. Hampton, E. Nyairo, Polymer (2005) 3014–3021.
[46] S.C. Zunjarrao, R. Sriraman, R.P. Singh, Journal of Material Science 41 (2006) 2219–2228.
[47] T.P. Mohan, M.R. Kumar, R. Velmurugan, Journal of Material Science 41 (2006) 2929–2937.
[48] B.B. Johnsen, A.J. Kinloch, R.D. Mohammed, A.C. Taylor, S. Sprenger, Polymer 48 (2006) 530–541.
[49] V. Nigam, D.K. Setua, G.N. Mathur, K.K. Kar, Wiley Interscience (2004).
[50] A. Yasmin, J.J. Luo, J.L. Abot, I.M. Daniel, Composites Science and Technology 66 (2006) 2415–2422.
[51] W.J. Choi, S.H. Kim, Y.J. Kim, S.C. Kim, Polymer 45 (2004) 6045–6057.
[52] S. Solarski, S. Benali, M. Rochery, E. Devaux, M. Alexandre, F. Monteverde, P. Dubois, Journal of Applied Polymer Science 95 (2005) 238–244.
[53] A. Yasmin, J.L. Abot, I.M. Daniel, Scripta Materialia 49 (2003) 81–86.
[54] Q.M. Jia, M. Zheng, C.Z. Xu, H.X. Chen, Polymers for Advanced Technologies 17 (2006) 168–173.
[55] J.F. Timmerman, B.S. Hayes, J.C. Seferis, Composites Science and Technology 62 (2002) 1249–1258.